Original Article

Evaluation of advanced refractories to replace water-cooled panels in steelmaking electric arc furnaces

Pedro Henrique Couto Almeida[1,2]*
Victor Carlos Pandolfelli[2]

Abstract

The electric arc furnace (EAF) process is gaining prominence in global steel production due to its lower CO_2 emissions and energy consumption. However, the continued use of water-cooled panels in the EAF upper sidewall presents serious safety risks, primarily due to the potential for water-steel interactions that may lead to explosions. Replacing these components with refractory panels can eliminate this risk while significantly reducing heat loss and water usage. This study evaluates five commercially available refractory castables using laboratory testing and thermodynamic simulations to determine their suitability for this application. An alumina-spinel (AM) castable emerged as the most promising material, offering an optimal balance of mechanical strength, thermal shock resistance, slag resistance, and refractoriness making it a strong candidate for safer and more efficient EAF operation.

Keywords: Refractory castables; Electric arc furnace; Panel.

1 Introduction

In steelmaking Electric Arc Furnaces (EAFs), one of the main factors behind operational disruption and potential accidents is the contact of cooling water from leakages of water-cooled furnace components with liquid steel. This combination (liquid steel and water) can generate an explosion and projection of liquid metal tens of meters away [1].

Water leakage from pressurized tubular cooling systems in the EAF can be caused by several factors: thermal overload arising from the electric arc or chemical energy used in the furnace process [1], cracks by thermal fatigue, errant arc strike or mechanical puncture during operation, generating holes [2]. Besides the resulting operational disruption and productivity loss, serious accidents can happen, as shown by the examples given in Table 1.

Water-cooled panels typically comprise the EAF upper sidewall above the slag line (Figure 1). They are held in a water-cooled cage which supports them. The furnace lower sidewall and bottom, on the other hand, consist of a steel shell with several layers of refractory lining [5]. Historically, the cooled panels were introduced in the 1970s to replace refractory bricks, which commonly fell when they lost support due to the wear in the slag line. The panels allowed for individual replacement with a minimum of downtime and decreased refractory consumption and damage to the furnace shell [5].

However, besides the risk of water leakage causing operational disruption and potentially serious accidents, the water-cooled panels worsen the energy balance and drastically increase the water consumption of the EAF. Typically, 5 to 10% of all the energy input to the EAF goes to the cooling water [5].

An alternative to overcome these disadvantages is the replacement of the water-cooled panels by refractory ones, that can be made with a similar metallic shell that can be attached to the EAF upper structure, such as proposed by SMS Siemag AG in the patent document EP 2 460 895 A2 [7] (Figure 2). The refractory panels have a refractory lining cast with a refractory castable instead of metallic tubes with flowing water.

This solution can lead to greater operational safety, reduced heat losses, increased furnace availability due to shorter times required for maintenance and replacement, reduced costs for storage of replacement parts (hoses, connections, measurement, etc.), and reduced investment costs [7].

Furthermore, there are advancements in the refractory castable technology that were introduced only in the past few decades. Some examples include magnesia or spinel-based compositions (that typically have higher resistance to corrosion by the EAF slags), new binder concepts, and additives that allow the engineering of the microstructure to control the final properties of the material [8]. These advancements have expanded the number of options that can be used and allowed the production of pre-cast refractory shapes with fine-tuned properties that can better fit challenging applications such as a panel in the EAF upper sidewall.

[1]*Centro de Pesquisa e Desenvolvimento, RHI Magnesita, Contagem, MG, Brasil.*
[2]*Programa de Pós-Graduação em Ciência e Engenharia de Materiais, Universidade Federal de São Carlos – UFSCar, São Carlos, SP, Brasil.*

**Corresponding author: pedro.almeida@rhimagnesita.com*
E-mail: vicpando@ufscar.br

Table 1. Sample listing of serious EAF accidents caused by water leakages [2-4]

Year	Country	Facility	Injuries	Description
2010	U.S.	Steel mill	1 killed, 4 injured	Leak in EAF caused water to mix with molten slag
2010	U.S.	Steel pipe manufacturing	1 killed, 2 injured	Workers exposed to 2000 F molten metal and steam in EAF explosion
2011	U.S.	Carbide manufacturing	2 killed, 2 injured	Water leak in EAF caused over-pressure event ejecting 3800 F furnace contents
2011	Australia	Steel mill	4 injured, 1 seriously	Water accidentally entered EAF as workers were removing partly melted scrap
2012	Canada	Steel mill	1 injured	Injury occurred from a small steam explosion in the melt shop EAF
2012	U.S.	Steel mill	2 injured	EAF steam explosion injured two workers
2013	U.S.	Steel mill	1 killed	EAF explosion fatally injured one worker
2013	U.S.	Steel mill	3 injured, 2 critically	Water leak into 3000 F EAF caused severe explosion
2013	Mexico	Steel mill	4 killed, 10 injured	Explosion occurred during routine maintenance at DRI intake of EAF
2014	U.S.	Steel mill	2 killed, 17 injured	Deaths and injuries resulted from violent EAF explosion
2014	U.S.	Steel mill	1 killed, 5 injured	Leak caused 1000 gallons of water to pour into EAF, creating a hydrogen explosion
2014	U.S.	Steel mill	1 killed	Pipe exploded in a BOP furnace, fatally injuring one worker
2016	U.S.	Steel mill	2 injured	Reaction in a 175-ton EAF triggered an explosion
2017	India	Steel mill	2 killed, 7 injured	Leakage of water caused a blast in a 20-tonne EAF
2021	U.S.	Steel mill	8 injured	There was a cooling system failure, and water was introduced in the EAF causing an explosion

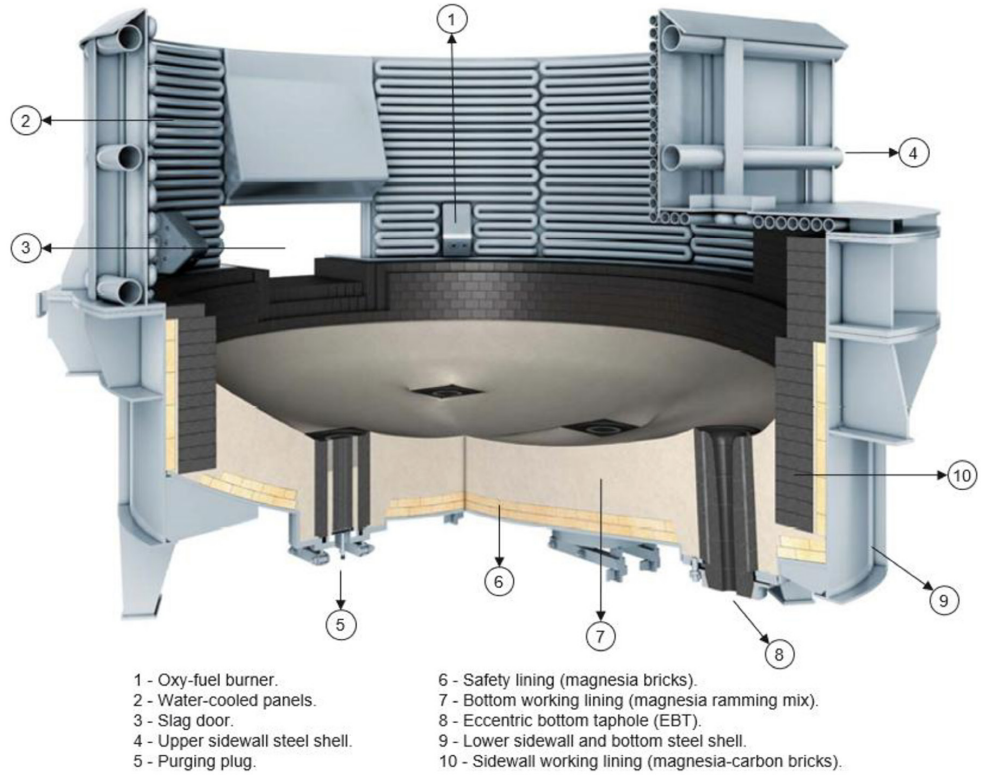

Figure 1. Typical EAF lining structure [6].

In application in the EAF, refractory panels would be exposed to several potential wear factors. During furnace charging, heavy and sharp scrap pieces can strike them. Also, the panels can be exposed to very high radiant heat fluxes coming from the electric arc. Additionally, slag may infiltrate/corrode the refractory because of slag splashing (due to the gas lances) and slag foaming. Considerable thermal cycling would also be present as the furnace roof is opened and buckets with cold scrap are fed into the furnace for each new heat. Hence the refractory castable should have an advanced formulation that allow for a good balance of the following properties: mechanical strength, refractoriness, slag corrosion and infiltration resistance and thermal shock resistance.

The objective of this work is to evaluate, among various technologies commercially available, the most appropriate refractory castable to be applied as working material for the described refractory panels, by using laboratory characterization and thermodynamic simulation.

2 Materials and methods

Five commercial refractory castables by RHI Magnesita were evaluated in this work. Their main features are summarized in Table 2.

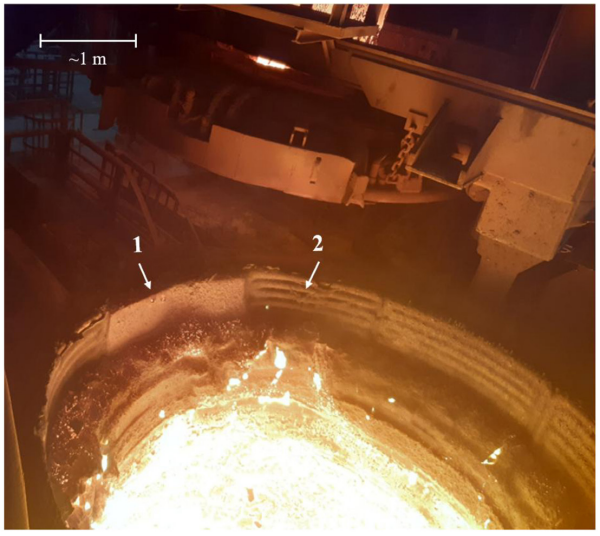

Figure 2. EAF upper sidewall with a refractory panel (1) replacing one of the water-cooled panels (2).

Testing specimens were prepared using a planetary mixer (Hobart HL600-1STD/SEG, 2 minutes dry-mixing, 5 minutes wet-mixing) and acrylic molds under vibration (MAVI UHDE at 40 Hz for 2 minutes). The specimens were cured for 24 hours at room temperature, demolded and dried at 350 °C for 6 hours. Three dried prismatic specimens (160 x 40 x 40 mm) of each composition were used to measure the modulus of elasticity (MOE, by the sonic method, according to NBR 13202-15 [9]), bulk density and apparent porosity (BD and AP, according to ASTM C830-00 [10]), cold crushing strength (CCS, according to NBR 11222-10) and chemical composition (by X-ray fluorescence – XRF – according to ISO 12677:11, results are shown in Table 3).

Thermal shock resistance was determined according to NBR 13202-15 [9], using ΔT=1200 °C and dwell time at this temperature of 30 min. MOE was measured at room temperature before the test and after 1, 2, 3 and 5 thermal shock cycles using the sonic method (NBR 13202-15 [9]).

Thermodynamic simulations were carried out using the software FactSage 8.1. The oxides that represented less than 0.3 wt.% (Table 3) were neglected and the resulting chemical compositions were used for calculations. The amount of liquid phase as a function of temperature was determined using the databases FactPS and FToxid. An ideal gas phase was considered, and the pressure was set at 1 atm. All pure solids and solid solutions were included, except for pseudobrookite (valid only under relatively reducing conditions) and titania spinel (valid only under relatively reducing conditions and for titanium-rich solutions). Temperatures between 1000 °C and 1800 °C were examined, with 20 °C steps and including transition points.

Slag tests were carried out in a laboratory rotary kiln (RK) heated with a natural gas torch, with one castable composition at a time, at 1650 °C for 2 hours. Six refractory specimens (trapezoidal prisms with 50 mm thickness) were used to assemble the internal lining of the RK, as illustrated in Figure 3. A slag sample from the EAF of a steelmaking partner was utilized. The chemical composition of the slag was analyzed using XRF (according to ISO 12677:11, results shown in Table 3). At the beginning, and after each 30 minutes, a new charge of slag (250 g) was added to the furnace. The remaining liquid slag was poured from the RK after each 30 minutes, before adding a new charge. After the test, specimens were cut longitudinally in half and the thickness variation (wear) and depth of slag infiltration were measured (six measurements for each specimen).

Table 2. Main features of the tested refractory castables

Castable	A	AM	ASC	M	MC
Aggregates	Sintered mullite, fused alumina	Tabular alumina, sintered spinel	Tabular alumina, sintered mullite	Sintered magnesia	Sintered magnesia
Binder	Calcium aluminate cement (low)	Calcium aluminate cement	Colloidal silica	Phosphate	Phosphate
Additives	Fumed silica, green chromium oxide	Reactive alumina	Silicon carbide, fine petroleum coke	Fumed silica	Fumed silica, graphite
Application	EAF delta roof	Steel ladle well blocks	Blast furnace runners	Tundish furniture	-

Table 3. Chemical composition of the refractory castables and the slag

wt.%	A	AM	ASC	M	MC	Slag
Al_2O_3	83.71	91.54	81.69	0.72	0.23	2.53
MgO	0.64	6.45	0.61	93.82	93.15	8.16
SiO_2	9.11	0.03	4.56	3.41	3.70	13.00
Cr_2O_3	2.08	-	0.03	0.01	0.01	11.54
Fe_2O_3	0.77	0.09	0.36	0.40	0.88	28.44
CaO	0.90	1.76	0.48	1.01	0.80	29.71
TiO_2	2.26	-	1.41	0.01	0.01	0.23
Na_2O	0.23	0.13	0.20	0.05	0.18	-
P_2O_5	0.14	-	0.05	0.49	0.75	0.23
MnO	0.02	-	0.02	0.08	0.29	5.68
ZrO_2	0.11	-	0.18	-	-	-
K_2O	0.03	-	0.04	-	-	-
V_2O_5	-	-	-	-	-	0.32
SO_3	-	-	-	-	-	0.17
SiC	-	-	10.38	-	-	-
Basicity (CaO/SiO_2)	-	-	-	-	-	2.29

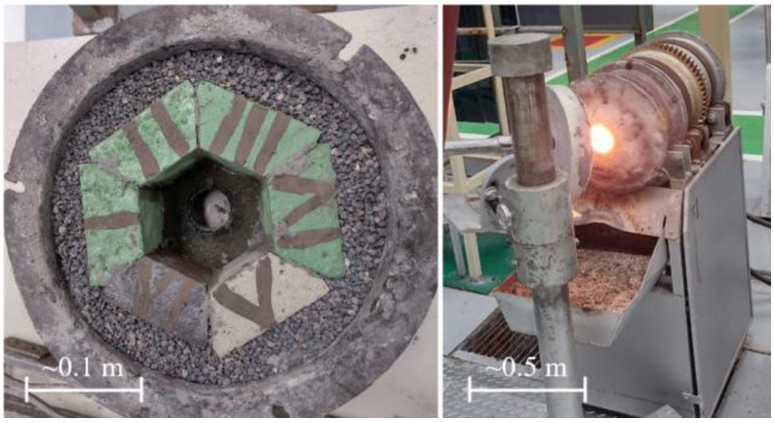

Figure 3. Rotary kiln slag test assembly (left) and running the test (right).

To complement the analysis, thermochemical and viscosity simulations were carried out using FactSage 8.1 (FToxid, FactPS and Melts databases) to assess liquid phase formation (amount and viscosity) for the interaction of refractory castables and slag (proportion of refractory from 0 to 1 with 0.05 steps) at 1650 °C.

3 Results and discussion

3.1 Thermal shock resistance and physical tests

The residual MOE of each castable composition as a function of the number of thermal shock cycles is presented in Figure 4. A lower residual MOE indicates that more cracks were generated in the material, and hence the mechanical damage increases [9].

Castable ASC presented the best thermal shock resistance, induced by the silicon carbide addition [8,11] and colloidal silica as binder [12]. Composition A had the second-best result, as it contained sintered mullite, which has high thermal stability and low thermal expansion [13], and because of its relatively low MOE and CCS (Table 4) [14].

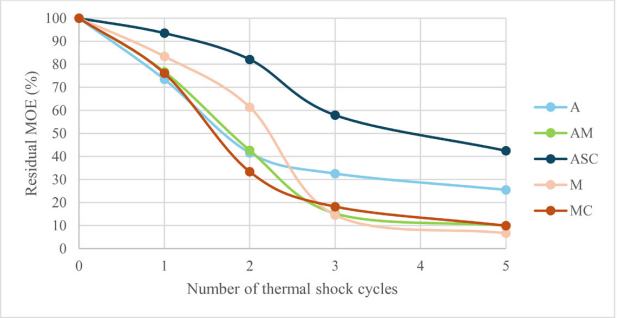

Figure 4. Residual MOE versus the number of thermal shock cycles (ΔT=1200 ºC; dwell time at this temperature: 30 min).

Castables AM, M and MC had similar results (Figure 4). Although alumina and spinel have lower thermal expansion

Table 4. Physical and mechanical properties after drying (350 °C/6h)

Property	A	AM	ASC	M	MC
AP (%)	16.0 ± 0.8	14.5 ± 0.2	14.3 ± 0.1	17.7 ± 0.4	18.8 ± 0.4
BD (g/cm³)	2.90 ± 0.02	3.05 ± 0.01	2.99 ± 0.01	2.73 ± 0.01	2.61 ± 0.01
MOE (GPa)	50 ± 3	110.5 ± 0.6	70.7 ± 0.4	54 ± 2	46 ± 2
CCS (MPa)	22 ± 2	75 ± 7	52 ± 2	58 ± 10	37 ± 3

Table 5. Wear and infiltration depth results from slag tests

Parameter	A	AM	ASC	M	MC
Wear [1] (%)	6.3 ± 1.1	5.7 ± 1.2	46.3 ± 6.1	1.4 ± 0.2	1.7 ± 0.5
Infiltration (%)	Max. 26.7	Max. 6.1	-	Max. 28.9	69.3 [2]
	Min. 26.2	Min. 4.1		Min. 25.9	
Total (%)	32.8	10.8	46.3	28.8	71.0

Notes: (1) Average and standard deviation of 6 testing specimens; (2) Only one specimen was measured.

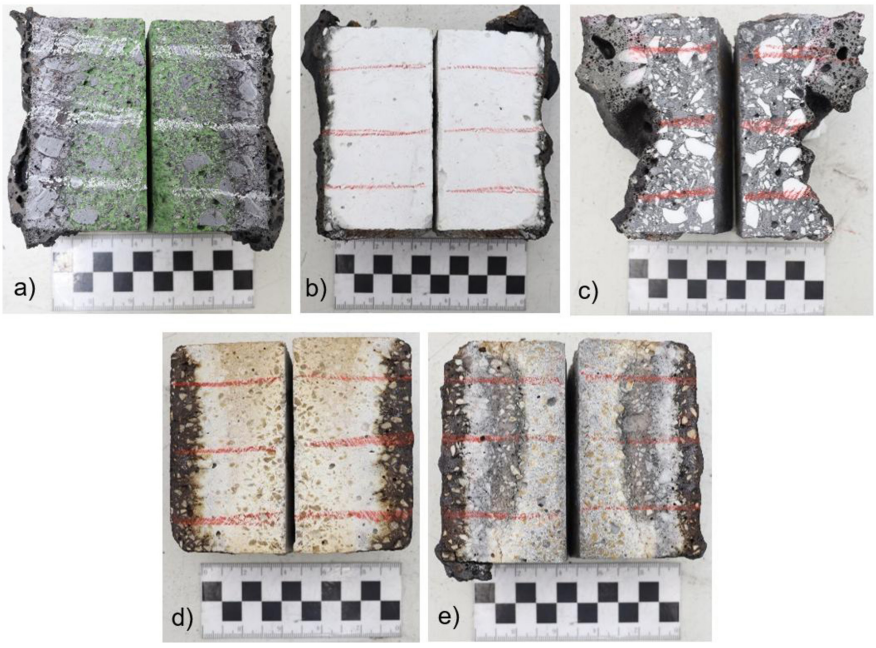

Figure 5. Longitudinal cross section after the slag test (hot face on the sides and cold face in the centre) of a representative specimen of castables a) A, b) AM, c) ASC, d) M and e) MC.

than magnesia [15], composition AM has higher MOE and CCS and lower porosity (Table 4), which decreased the thermal shock resistance [14]. Additionally, the use of graphite did not improve the behavior of MC, probably due to fast oxidation at 1200°C [16].

3.2 Slag tests and thermodynamic simulation

The longitudinal cross-section of a representative specimen of each refractory castable, after the slag test, with the hot face on the sides and cold face in the center, is shown in Figure 5. Wear and infiltration depth results are presented in Table 5. Wear values are in good agreement with thermodynamic simulation (Figure 6).

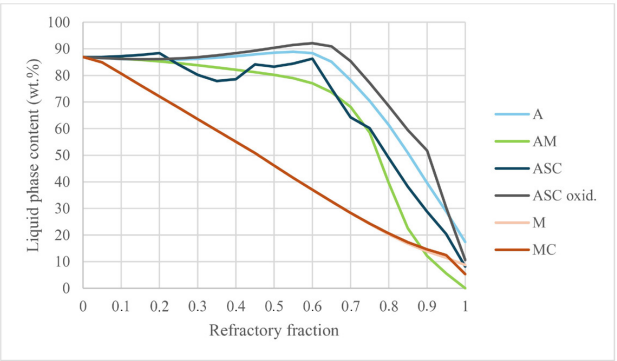

Figure 6. Liquid phase content versus refractory fraction in the interaction of refractory castables and slag at 1650 °C (simulated with FactSage 8.1).

Table 6. Key properties and values of the respective indicators for each refractory castable

Property	Indicator	A	AM	ASC	M	MC
Mechanical strength	CCS after drying (350 °C/6h)	22	75	52	58	37
Thermal shock resistance	Residual MOE (%) after 5 thermal shock cycles (ΔT=1200 °C; dwell time at this temperature: 30 min)	25.5	10.0	42.5	6.7	9.9
Refractoriness	Total content of solid phases (wt.%) at 1650 °C from thermodynamic simulation using FactSage 8.1	82.6	100.0	91.8	91.2	94.5
Slag corrosion resistance	100% minus average wear in slag tests	93.7	94.3	53.7	98.6	98.3
Slag infiltration resistance	100% minus average infiltration in slag tests	73.5	94.9	100.0	72.6	30.7

Compositions leading to the formation of more liquid phases in the interaction with the slag were more corroded in the test. In the case of ASC, wear was significantly higher than in the other castables, probably due to SiC active oxidation at 1650 °C [17]. Thermodynamic and viscosity simulations were repeated for ASC considering the transformation of SiC to SiO_2 ("ASC oxid." in Figures 6 and 7), indicating a higher liquid phase formation in the interaction with the slag.

For compositions ASC, AM, M and MC, infiltration depth (Table 5) can be partially associated with the porosity (Table 4) and mainly with the viscosity of the liquid that is formed in the interaction with the slag (Figure 7). A more porous material in contact with a liquid phase with low viscosity tends to be more infiltrated.

In the case of composition A, infiltration was high despite the elevated viscosity of the formed liquid, due to their amount (Figure 6) and the porosity of the castable.

Graphite addition was expected to result in a lower wear and infiltration in composition MC when compared to M, because of its low surface energy, which makes it non-wettable by the molten oxides that comprise the slag [18]. However, this was not observed, probably due to the oxidation of graphite [16] and the higher porosity of castable MC (Table 4).

Liquid phase content as a function of temperature for the refractory castables and for composition ASC considering the transformation of SiC to SiO_2 ("ASC oxid.") are presented in Figure 8. Castable AM has the highest refractoriness, with liquid phase formation starting only at ~1780 °C. The magnesia formulations (M and MC) present the lowest solidus, ~1150 °C, due to phosphate containing phases, but display lower liquid content at higher temperatures (e.g., 1650 °C) than compositions A and ASC (considering the oxidation of SiC).

3.3 Combined analysis

The main properties of the refractory castable that are expected to affect performance are summarized in Table 6. One indicator from laboratory tests was selected for each property, and the respective values for the studied castables are presented in Table 6.

The values in Table 6 were normalized in a range of 10 to 100 and used to assemble the radar chart in Figure 9. The castable that presented the best combination of the key properties is AM. It has the highest mechanical strength and

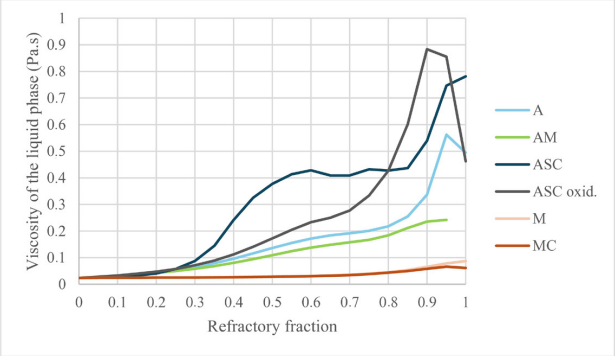

Figure 7. Viscosity of the formed liquid phase versus refractory fraction at 1650 °C (simulated with FactSage 8.1).

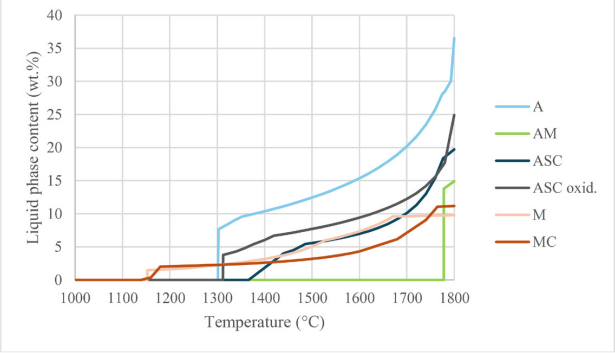

Figure 8. Liquid phase content versus temperature for the refractory castables (simulated with FactSage 8.1).

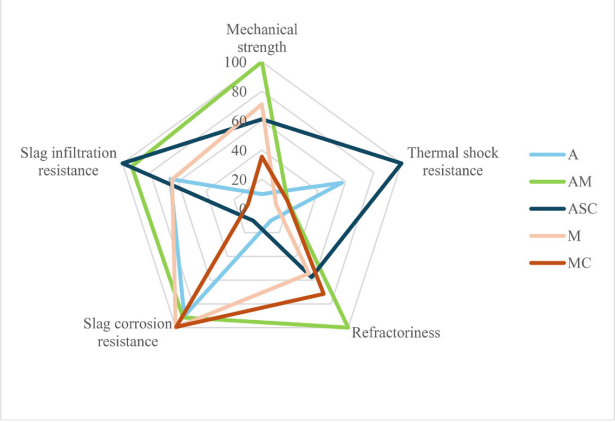

Figure 9. Radar chart of normalized values for key properties.

refractoriness, the second-best infiltration resistance, a corrosion resistance that is lower than the magnesia compositions but higher than the alumina ones, and a thermal shock resistance that is at least equal or higher than the magnesia castables.

4 Conclusion

This study systematically assessed five commercial refractory castables for potential use in replacing water-cooled panels in electric arc furnaces (EAFs). Among the candidates, the alumina-spinel (AM) castable has shown the best overall performance, combining high mechanical strength, superior slag infiltration resistance and excellent refractoriness.

These qualities position it as a viable and safer alternative to conventional water-cooled components, with the added benefits of reduced energy loss and water consumption. Future research should prioritize in-situ testing, post-mortem analysis and long-term performance evaluations to support industrial adoption and further enhance EAF sustainability and safety.

Acknowledgements

This study was financed in part by the Coordenação de Aperfeiçoamento de Pessoal de Nível Superior - Brasil (CAPES) - Finance Code 001. The authors are also thankful to RHI Magnesita for supporting this research.

References

1 Silva JNA. Estudo Teórico e Experimental do Efeito do Ciclo Térmico no Painel Refrigerado de Forno Elétrico a Arco [thesis]. Curitiba: Universidade Federal do Paraná; 2014.

2 Ferguson S, Zsamboky N. Electric Arc Furnace (EAF) Explosions: A Deadly but Preventable Problem. Iron Steel Technol. 2017;14(1):30-35.

3 Gupta J. Water leakage may have caused blast at Metal and Steel Factory [Internet]. New Delhi: The Times of India; 2017 [cited 2025 May 2]. Available at: http://timesofindia.indiatimes.com/articleshow/57634451.cms?utm_source=contentofinterest&utm_medium=text&utm_campaign=cppst

4 Goldstein J. Electric arc furnace explosion at Pueblo, Colorado steel mill leaves eight workers seriously injured [Internet]. Oak Park: World Socialist Web Site; 2021 [cited 2025 May 2]. Available at: https://www.wsws.org/en/articles/2021/06/03/pueb-j03.html

5 Bowman B, Jones JAT, LeFrank PA. Electric Furnace Steelmaking. In: Fruehan RJ, editor. The Making, Shaping and Treating of Steel: Steelmaking and Refining Volume. Pittsburgh (PA): The AISE Steel Foundation; 1998. p. 525-60.

6 Wucher J. FEA Manual de Instalação: Revestimento de um Forno Elétrico a Arco. Internal document. Vienna: RHI Magnesita; 2018.

7 Bültena R, Ertl M. Metallurgisches Gefäß, insbesondere Elektrolichtbogenofen. European Patent EP 2 460 895 A2. 2011 Jun 12.

8 Luz AP, Braulio MAL, Pandolfelli VC. Refractory castable engineering. Baden: Göller Verlag; 2015.

9 Associação Brasileira de Normas Técnicas. ABNT NBR 13202: Materiais refratários – Determinação do choque térmico pelo módulo de elasticidade residual (Refractory materials – Determination of thermal shock by residual modulus of elasticity). Rio de Janeiro: ABNT; 2015.

10 ASTM C830. Standard Test Methods for Apparent Porosity, Liquid Absorption, Apparent Specific Gravity, and Bulk Density of Refractory Shapes by Vacuum Pressure. 2000.

11 Zhang W, Dai W, Chiyoda N. Research on thermal shock resistance of mullite-bauxite-silicon carbide castable refractory. Chinese Journal of Geochemistry. 2012;31:204-208.

12 Sarkar R. Binders for Refractory Castables: An Overview. Interceram. 2020;69:44-53.

13 Lima LKS, Silva KR, Menezes RR, Santana LNL, Lira HL. Microstructural characteristics, properties, synthesis and applications of mullite - A review. Cerâmica. 2022;68:126-142.

14 Schacht CA. Refractories handbook. Pittsburgh (PA): CRC Press; 2004.

15 Braulio MAL, Rigaud M, Buhr A, Parr C, Pandolfelli VC. Spinel-containing alumina-based refractory castables. Ceramics International. 2011;37:1705-1724.

16 Jiang W, Nadeau G, Zaghib K, Kinoshita K. Thermal analysis of the oxidation of natural graphite – effect of particle size. Thermochimica Acta. 2000;351:85-93.

17 Vaughn WL, Maahs HG. Active-to-Passive Transition in the Oxidation of Silicon Carbide and Silicon Nitride in Air. Journal of the American Ceramic Society. 1990;73:1540-1543.

18 Bitencourt CS, Pandolfelli VC. Carbon containing refractories: properties, characteristics and variables in their composition. Cerâmica. 2013;59:84-114.

Received: 17 Out. 2025
Accepted: 24 Nov. 2025

Editor-in-charge:
André Luiz Vasconcellos da Costa e Silva